ELSEVIER

Journal of Nuclear Materials 281 (2000) 171–181

journal of nuclear materials

www.elsevier.nl/locate/jnucmat

Investigation on the zirconia phase transition under irradiation

D. Simeone [a,*], J.L. Bechade [b], D. Gosset [a], A. Chevarier [c], P. Daniel [d], H. Pilliaire [e], G. Baldinozzi [f]

[a] *SEMI, Lab. d'Etudes Materiaux Absorbents, CEA, CE Saclay, F-91191 Gif sur Yvette cedex, France*
[b] *SRMA, CEA, CE Saclay, F-91191 Gif sur Yvette cedex, France*
[c] *IPNL, IN2P3, F-69100 Villeurbanne cedex, France*
[d] *Laboratoire de Physique de l'Etat Condensé, UPRES A CNRS n°6087, F-72085 Le Mans cedex, France*
[e] *Societé INEL, F-45410 Artenay, France*
[f] *Laboratoire de chime Physique du solide, URA CNRS 453, F-92295, Chatenay Malabry cedex, France*

Received 10 March 2000; accepted 22 June 2000

Abstract

Zirconia, ZrO_2, produced by the oxidation of zirconium alloys in nuclear reactors, possesses a high stability under neutron irradiation. No amorphisation of yttrium-stabilised zirconia has been observed even at high dpa values (≈ 100 dpa). In pure monoclinic zirconia, a phase transition monoclinic $\rightarrow$ cubic (tetragonal) induced by irradiation has already been observed. The aim of this work is to study in detail the mechanism responsible for this transition. For that purpose, different kinds of irradiations with electrons (to study point defects) and low energetic ions (to study clusters due to collision cascades) have been performed on zirconia samples. A local probe (Raman spectroscopy) and a non-local probe (grazing X-ray diffraction) have been used to characterise the phase formed during irradiation, which is clearly the tetragonal phase. For the ionic implantation, the grazing X-ray diffraction permits to separate effects due to the ballistic collisions and the implantation peak. Using this method, it was possible to show that the profile of the tetragonal phase was only linked to the dpa profile. This result associated to the results obtained by the Raman spectroscopy (broadening of Raman peaks) shows that the phase transition may be induced by clusters formed near the collision cascades.

1. Introduction

Under operating conditions in Pressurized Water Reactor (PWR), the zirconium alloys, used as cladding and structural elements of the nuclear fuel assembly, are oxidized creating a zirconia layer which modifies their mechanical behaviour under irradiation. This point associated to the high stability of zirconia under irradiation leads us to study this material with a great attention. Moreover, the knowledge of the crystal structures of different zirconia polymorph and the transition mechanism between them are of considerable interest in view of their connection with the properties of advanced zirconia based ceramics.

In this paper, we focus our attention on the evolution of pure zirconia under ions irradiation. The effects of impurities, which are present in the zirconia layer formed during the oxidation of Zr alloys in a nuclear reactor may stabilise the zirconia phases produced. These effects are not studied here. Moreover, the influence of temperature on zirconia behaviour under irradiation is not the scope of this work. Only irradiations at room temperature were done.

Previous works on the zirconia crystallographic structure have revealed the existence of several polymorphs of ZrO_2 in different ranges of temperatures and pressures. At atmospheric pressure and at room temperature, the monoclinic C_{2h}^5 phase (associated to the non-symorphic $P2_1/c$ space group) is stable [1]. Around

* Corresponding author. Present address: Centre d' Étude de Saclay, Laboratoire de Metallurgie et de Microscopie Electronique, CEA, 911191 Gif sur Yvette cedex, France. Tel.: +33-1-69 08 29 20; fax: +33-1-69 08 90 82.
E-mail address: david.simeone@cea.fr (D. Simeone).

0022-3115/00/$ - see front matter
PII: S0022-3115(00)00183-5

1400 K, a phase transition occurs and the crystal becomes a tetragonal D_{4h}^{15} structure ($P4_2/nmc$) [2]. Near 2600 K, a second phase transition leads to the cubic O_h^5 structure ($Fm3m$) [3]. The mechanism describing the m → t phase transition is not clear [4]. Some authors have attempted to study the m → t phase transition using the group theory formalism [5–7]. According to them, a classical Landau free energy is not able to describe correctly the displacive m → t phase transition. Under irradiation, the problem is more complicated and no prediction on an eventual phase transition has been made. However, under neutron and ion irradiation at low temperatures (<1000 K) and under atmospheric pressure, a m → c(t) phase transition has been observed [8].

The aim of this paper is to study this phase transition under irradiation. For that purpose, we have irradiated pure monoclinic zirconia pellets with electrons, 800 keV Bi and O ions at different fluences at room temperature. Such experiments permit to analyse the phase transition in terms of point defects production (irradiation by electrons) or in terms of extended defects due to ballistic collisions (irradiation by ions). On implanted pellets, grazing X-ray diffraction permits to follow the phase transformation as a function of the depth, and the Raman spectroscopy is able to detect different zirconia crystallographic forms induced in this case by irradiation. This probe gives useful information on the local potential associated to different ions in this insulator.

2. Experimental procedure

These irradiations follow the work of Sickafus et al. [8], who have irradiated monoclinic zirconia powders with 340 keV Xe at 120 K. A phase transition from monoclinic to cubic (or tetragonal) phase has been observed under this irradiation for fluences above 5×10^{14} cm^{-2}. However, classical X-ray diffraction measurements do not separate effects due to the compression of zirconia lattice induced by Xe implantation and/or to clusters due to ballistic cascades. To study the evolution of the phase transition induced by different kinds of ions, splitting effects due to atomic collisions and implantation of projectiles, grazing X-ray diffraction has been used. Moreover, Raman scattering has been used to separate different zirconia phases which possess very separate signatures.

2.1. Samples preparation

A zirconia powder with a purity of 99.97%, produced by Alpha Aesar Company, was sintered 15 min at 2123 K in a graphite furnace under hot pressing (2×10^6 Pa). During the natural cooling, the pressure was maintained. This sintering process permits to obtain high-density pellets. These pellets were cut to obtain pure zirconia discs (with a diameter of 12 mm and a thickness of 1 mm) with a density equal to 95% of the theoretical density (5.83 g cm^{-3}). These discs were heated at 1073 K during 24 h in air to obtain the correct stochiometry of zircionia. The grain size of the pellets, measured by optical metallography, was about 10 μm. Samples were polished until 0.5 μm to collect accurate X-ray diffraction diagrams under grazing incidence. To assess the quality of ZrO_2 samples, X-ray diffraction experiments were carried out on an Inel X-ray diffractometer. Samples were only composed of the monoclinic phase of ZrO_2 (cf. Fig. 1). The lattice parameters of all pellets were found to be in agreement with the expected stoichiometry [1]. No Bragg shifts have been observed on the X-ray diffraction diagram. This implies that no macroscopic stresses are present in the material after the heating treatment. Moreover, in order to check that no crystallographic preferential orientations appear, a pole diffraction figure has been performed. No crystallographic texture has been observed.

As low energetic ions (800 keV) are used in this study, their penetration depths are small (0.6 μm for O and 0.1 μm for Bi). To separate effects due to ballistic collisions from those due to the creation of implanted profiles on the phase transition, X-ray diffraction with a variable penetration depth must be used. That is the reason why grazing incidence has been used. Based on the formalism developed by Vineyard [9] and Brunel [10], it is possible to select τ, the penetration depth of X-ray in zirconia, by selecting different grazing incidences and to compute also a pseudo-structure factor $F(\alpha, hkl)$. The Inel grazing diffraction setup was optimized to obtain a correct grazing X-ray incidence according to the following points:

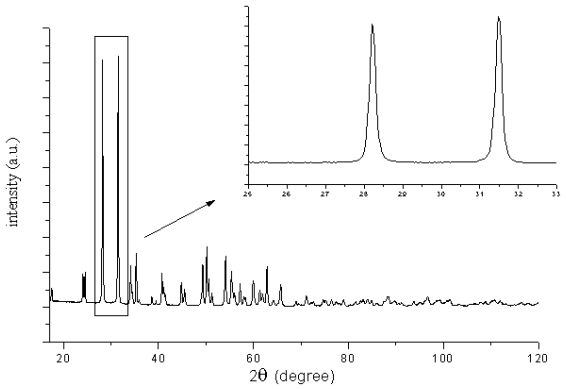

Fig. 1. X-ray diffraction spectra of pure monoclinic zirconia pellets obtained by hot pressing sintering. The zoom clearly shows that no other zirconia phases are produced during the elaboration of pellets. Moreover, the analysis of the diffraction diagram exhibits no shift of the Bragg angles. Then we deduce that no residual stresses are produced during the elaboration.

A parallel optic (CuKα1, a flat Ge[1 1 1] monochromator and a crossed slits system). The sample is set on a spinning goniometer head, and the height to adjust the sample positioning is controlled by an accurate Z adjustment using an in-situ microscope. A dedicated sample delimiter allows to record only a small area (0.6 mm^2) of the diffracted surface on the sample. The Inel Curved Position Sensitive detector allows the simultaneous detection of diffracted beams over a 120° angular range.

Lattice parameters associated to monoclinic, cubic and tetragonal phases generate quite similar diffraction diagrams (except one peak). It is then difficult to dissociate the tetragonal and cubic phases on an X-ray diffraction diagram. In the Raman spectroscopy, the collected signal is due to interactions between photons and phonons, i.e. vibrations of atoms composing the unit cell. Then, this method appears as a powerful technique to detect the crystallographic changes and to discriminate between two neighboured structures as a function of the changes in group theory selection rules [11–13]. Moreover, the Raman spectroscopy is sensitive to the average short range order (electrostatic potential associated to the local environment of atoms) on the analysed surface (the penetration depth of the laser beam is about 3 μm for the selected wavelength) whereas X-ray diffraction is sensitive to the long range order (coherent diffraction due to extended defects). The Raman spectra of the Bi irradiated ZrO_2 samples were recorded in a back-scattering configuration, under microscope, by using a T64000 Jobin–Yvon ISA multichannel Raman spectrometer with a CCD detector. A confocal hole coupled with the microscope was adjusted to its minimum value in order to enhance the signal coming from the irradiated surface. The 514.5 nm and 488 nm excitation laser lines used (coherent argon–krypton ion laser) were tested together on the samples, in order to avoid the luminescence signal due to impurities (Bi atoms implanted). A Laser beam power not exceeding an approximate level of 20 mW was chosen. It was checked that the surface of the samples was not damaged by the Laser beam light. Moreover, the Raman spot size is about 5 μm and inferior to the grain size. This local probe then permits to study the phase transition in a grain considering it as a crystal.

2.2. Samples irradiation

Three different types of irradiation, at room temperature, were performed for our analysis of the elementary mechanism inducing the phase transition. To calculate the number of atoms displaced and the displacement per atom (dpa) induced by electrons, Bi and O ions, displacement threshold energies of 20 eV for zirconium and 60 eV for oxygen have been used based on previous works done on Al_2O_3 [14]. These values are certainly unrealistic but permit to compare roughly dpa induced by each projectile. Table 1 shows the variation of the displacement cross-section, calculated using the full cascade option of TRIM-98, induced by Bi (800 keV), O (800 keV) and Xe (340 keV) as a function of oxygen threshold in ZrO_2. Because the variation of the displacement cross-section as a function of the oxygen threshold is not negligible, the dpa thresholds observed in the following give only qualitative information. Therefore, dpa values calculated from these threshold energies clearly permit to compare different irradiations. The number of displaced atoms and the implantation profiles of Bi and O atoms calculated using TRIM-98 are presented in Figs. 2(a) and (b).

Under an electron beam: Samples were irradiated at 303 K by 2.5 MeV electrons at two different fluences (1.8×10^{18} and 1.8×10^{19} cm^{-2}). The penetration of electrons in a monoclinic zirconia target is about 2.5 mm.

Table 1
Number of defects, mean penetration depth straggling and displacement cross-section calculated by TRIM-98 as a function of oxygen thresholds

Ed_{Zr}	Ed_O	Number of shoots	Number of defects	Mean penetration depth (Å)	Straggling (Å)	Displacement cross sections (10^{-14} cm^2)
800 keV Bi ions						
20	60	100	5080	1074	315	1.6 ± 0.32
20	40	100	5290	1067	309	1.7 ± 0.335
20	20	100	9180	1064	309	3 ± 0.3
800 keV O ions						
20	60	100	780	6800	1179	$(4.06 \pm 0.81)10^{-2}$
20	40	100	940	6749	1250	$(4.88 \pm 0.97)10^{-2}$
20	20	1000	1420	6757	1261	$(7.38 \pm 1.48)10^{-2}$
340 keV Xe ions						
20	60	100	2420	710	199	1.18 ± 0.24
20	40	100	2920	709	220	1.43 ± 0.29
20	20	100	4380	710	220	2.14 ± 0.43

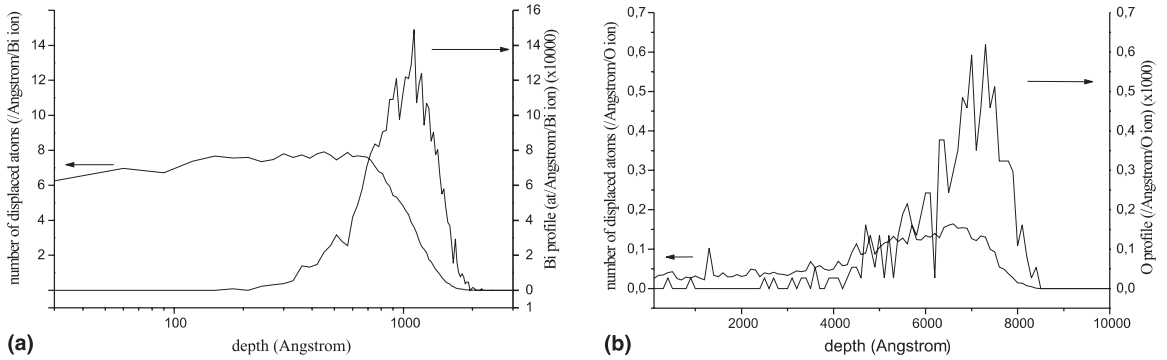

Fig. 2. (a) Dpa and implantation profile of Bi ions in zirconia (5.83 g cm^{-3}). This calculation was obtained using the program TRIM-98 and the dpa curve is calculated supposing that the displacement threshold energies of target Zr and O atoms are equal to 20 and 60 eV, respectively. (b) Dpa and implantation profiles of O ions in zirconia (5.83 g cm^{-3}). This calculation was obtained using the program TRIM-98 and the dpa curve is calculated supposing that the displacement threshold energies of target Zr and O atoms are equal to 20 and 60 eV, respectively.

Then all electrons pass through samples during the irradiation. These bombardments produce 4×10^5 and 4×10^4 dpa only due to electron atoms elastic collisions. It was not possible to define the production rate of defects induced by electronic excitations. Some results which should be confirmed [16] suggest that the rate production of point defects due to electronic collision could be 10^3 higher than dpa induced by elastic collision.

Under a Bi^{2+} beam: 5 samples were irradiated by 800 keV Bi ions at fluences varying from 10^{13} to 10^{15} cm^{-2} at 303 K. The average penetration depth of Bi ions is equal to 0.1 μm with a broadening equal to 0.031 μm. This implies that the total atomic fraction of Bi in the implantation peak vary from 1.8×10^{-5} to 1.8×10^{-3} for fluences varying from 10^{13} to 10^{15} cm^{-2}. The displacement cross-section induced by the 800 keV Bi penetration in the matrix has been calculated taking into account defects induced by cascades obtained by TRIM-98 and is equal to 1.6×10^{-14} cm^2. Then the total dpa profile in the samples is a linear function of the fluence and varies from 0.16 to 16. The interest of such an irradiation is that compact cascades are created. Then the probability to generate small clusters is important.

Under a O^{2+} beam: 5 samples were irradiated at fluences varying from 10^{13} to 10^{15} cm^{-2} by 800 keV O ions at 303 K. The average penetration depth of O ions in monoclinic zirconia targets is equal 0.6 μm with a broadening equal to 0.11 μm. This implies that the atomic fraction of O atoms in the implantation peak varies from 4.9×10^{-6} to 4.9×10^{-4} for fluences varying from 10^{13} to 10^{15} cm^{-2}. The displacement cross-section induced by the 800 keV O penetration in the matrix has been calculated taking into account defects induced by cascades obtained by TRIM-98 and is equal to 4×10^{-16} cm^2. Then the dpa vary from 4×10^{-3} to 4×10^{-1}. The interest of such an irradiation is that the cascades that are created are isolated one from each others. Then the probability to generate small clusters is low.

For both O and Bi irradiations, the total fractions of Bi and O atoms implanted in the matrix are not sufficient to stabilise the tetragonal phase. All effects, studied in the following paragraphs, will only be associated to physical effects induced by irradiation. Moreover, at these kinetic energies, the energy loss inside the zirconia matrix is mainly due to the nuclear stopping power.

3. Results and discussion

3.1. Effects produced by irradiation

3.1.1. Electron irradiation

Under an irradiation by electrons, no difference between the non-irradiated and the most irradiated zirconia samples have been observed on X-ray diffraction spectra (cf. Fig. 3). No phase transition is induced by electrons at room temperature and for such fluences. Electrons depose little energy in the zirconia insulator samples but generate many coloured centers [15]. In fact, before electron irradiations, zirconia samples are white and, after irradiation, samples become grey for a low electron fluence (1.8×10^{18} cm^{-2}), and black for a higher fluence (1.8×10^{19} cm^{-2}). This seems to show that these point defects do not affect on a long range order the zirconia phase transition. A comparison between Raman spectra collected on non-irradiated and electron irradiated samples (1.8×10^{19} cm^2) clearly shows no phase transition. Therefore, experiments at higher fluences must be done to confirm this point.

3.1.2. Oxygen and bismuth irradiation

After O and Bi irradiations, different incidence angles have been selected to probe irradiated samples at

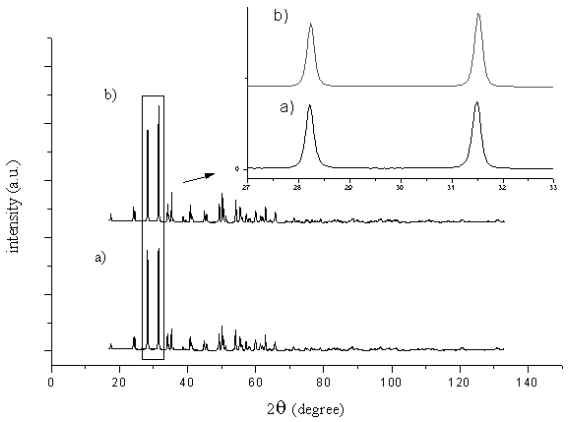

Fig. 3. Comparison between the non-irradiated (a) and the most irradiated electrons irradiated zirconia sample (b). No difference between the two X-ray diffraction peaks is observed. No new phase is induced by electrons irradiation at such fluences and at room temperature.

different thicknesses using the grazing X-ray diffraction (Fig. 4). Table 2 presents the different incidences and thicknesses associated with these experiments. The interest of selecting such depths is that they permit to separate the effects induced by collisions between the projectile ions and the target ions (dpa) and the effects due to the implanted ions (compression of the unit cell).

Under O irradiation, different X-ray diffraction spectra have been collected for different fluences (10^{13}, 5×10^{13}, 10^{14}, 5×10^{14} and 10^{15} ions cm^{-2}). On these spectra, no phase transition has been observed. Fig. 5 presents the collected X-ray diffraction spectra of the most irradiated zirconia sample. No peaks appears near $2\theta_{101t} = 30.17°$. This analysis is confirmed by the analysis of Raman spectra which does not show any peak of the tetragonal (or cubic) zirconia phase.

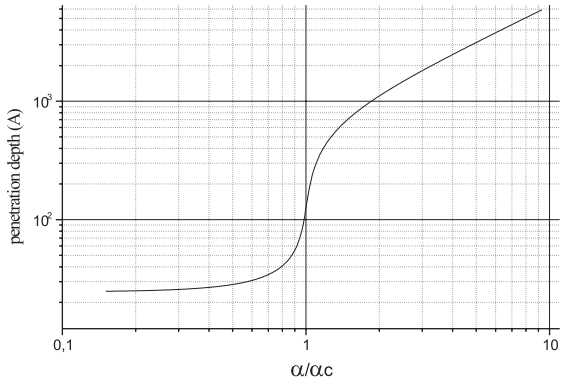

Fig. 4. Evolution of the depth penetration of X-ray as a function of the incident angle in grazing X-ray diffraction. This calculation was done with a critical angle equal to 0.332° and for the CuKα1 copper radiation.

Table 2
Grazing incidence angles as a function of the depth in a zirconia matrix. This calculation was done for the CuKα1 copper radiation with a critical angle equal to 0.332°

Bi projectile		O projectile	
Incident angle (°)	Depth (Å)	Incident angle (°)	Depth (Å)
0.3	50	0.5	1000
0.4	600	1.3	4000
0.5	1000	2	6000
0.8	2000	3	8000

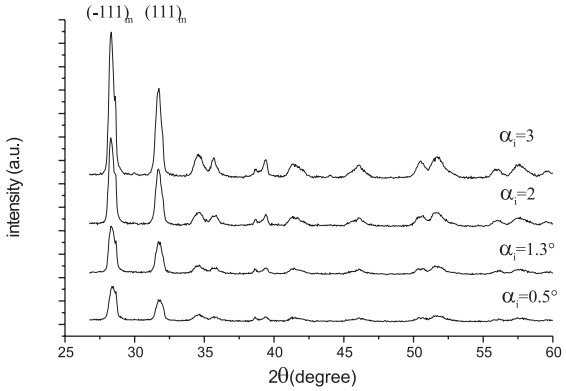

Fig. 5. X-ray diffraction spectra of zirconia samples irradiated by oxygen atoms for a fluence of 10^{15} ions cm^{-2}. No new phase appears on the spectra.

Under Bi irradiation, grazing X-ray diffraction shows a second phase, which is present in the monoclinic zirconia matrix. The average value of this second phase $\langle c_t(x) \rangle$, as a function of the analysed depth x, appears clearly for low X-ray penetration depths before the projectile ions are stopped in the target (cf. Fig. 2(a)). Fig. 6 exhibits the evolution of the new phase as a function of the depth in the matrix for the most irradiated sample. Such a new phase has also been observed using a Raman microprobe at different points of the irradiated surface. This new phase is studied in detail using a local probe (Raman spectroscopy) and a non-local one (grazing X-ray diffraction) in the following sections.

3.2. Raman spectroscopy analysis on Bi implanted samples

The collected Raman spectra associated to the cubic zirconia phases (fluorite structure) possesses only one peak situated near 607 cm^{-1}, whereas Raman spectra associated to the tetragonal phase is described by 7 peaks [11–13], one of which is located at 257 cm^{-1}. This peak is well separated from the 15 peaks induced by the

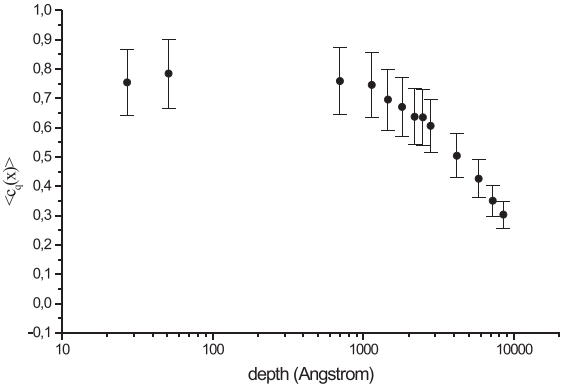

Fig. 6. Evolution of the tetragonal zirconia phase as a function of the depth in the most irradiated sample (this sample is irradiated by 800 keV Bi ions).

monoclinic phase. Then the distinction between the three phases can easily be obtained by Raman spectroscopy, without any ambiguity.

The number of lattice vibrations of different zirconia structures are well-known from group theoretical investigations [6]. The crystal stability of different zirconia comes from short-range interactions, which are assumed to be the sum of two body axially symmetric interactions limited to neighbours and long range electrostatic interactions. Using a Rigid Ion model, forces constants due to short-range interactions have been used to calculate lattice vibration [17]. Neglecting Zr–Zr short range interactions, O–O and O–Zr short range interactions are described by a couple of parameters (A_{ij}, B_{ij}) chosen to be the derivative of the short range potential V_i parallel and perpendicular to the line joining the interacting atoms:

$$A_{ij} = \frac{2\Omega}{e}\left(\frac{\partial^2 V_i}{\partial r_{ij}^2}\right),$$

$$B_{ij} = \frac{2\Omega}{e}\left(\frac{1}{r_{ij}}\frac{\partial V_i}{\partial r_{ij}}\right).$$

In these relations, Ω is the volume of the unit cell, e the electron charge and r_{ij} the distance between atoms i and j.

According to estimated values of Zr–O and O–O bonds, as given in Table 3, it has been possible to simulate Raman frequencies associated to the monoclinic phase in quite a good agreement with experimental peaks of Raman spectra collected on the most irradiated sample (Table 4). Besides, Raman peaks associated to this phase are not broadened by irradiation. These results show that defects due to irradiation seem to weakly perturb the interatomic local potentials around atoms on the monoclinic phase.

Three broadened peaks (cf. Table 5) clearly appear at 166, 257 and 586 cm^{-1} (Fig. 7). To index these Raman peaks, Raman spectra of the cubic (Fm3m), the tetragonal ($P4_2/nmc$) and high-pressure orthorhombic phases (Pnam and Pbca) have been calculated [18]. Experimental peaks obtained on irradiated samples can clearly be indexed only by the tetragonal phase (cf. Table 4) in agreement with X-ray diffraction spectra.

As the same tetragonal phase is observed at different grains (the laser spot is inferior to the grain size) of the irradiated surface (10 measures), we conclude that the

Table 3
Force constants A_{ij} and B_{ij} derived from [16] and bond lengths associated to Zr–O and O–O bonds in monoclinic and tetragonal phases. The positions of atoms used to compute the atomic bonds distances can be found in [1] for the monoclinic phase and in [2] for the tetragonal phase

Monoclinic				Tetragonal			
Sites	Bond lengths (Å)	A_{ij}	B_{ij}	Sites	Bond lengths (Å)	A_{ij}	B_{ij}
Zr–O1	2.048	2.89	−0.29	Zr–O1	2.07	2.74	−0.26
Zr–O2	2.050	2.88	−0.29	Zr–O1	2.47	0.57	0.03
Zr–O2	2.055	2.83	−0.28	O1–O1	2.65	0.48	−0.08
Zr–O1	2.139	2.26	−0.17	O1–O1	2.67	0.47	−0.07
Zr–O2	2.153	2.16	−0.16	O1–O1	3.24	0.18	0
Zr–O1	2.162	2.11	−0.15				
Zr–O1	2.165	2.09	−0.14				
Zr–O2	2.254	1.55	−0.10				
Zr–O2	2.272	1.45	−0.06				
Zr–O1	2.538	0.55	−0.10				
Zr–O2	2.588	0.52	−0.10				
Zr–O1	2.592	0.51	−0.009				
Zr–O1	2.606	0.50	−0.08				
Zr–O1	2.656	0.47	−0.07				
O3–O2	2.700	0.44	−0.06				

Table 4
Comparison between calculated frequencies (from [11]), IR and experimental frequencies obtained using force constants derived from [16]. The Raman frequencies associated to the tetragonal phase observed on the Raman spectrum are presented in bold

Monoclinic			Tetragonal			
Calculation (cm^{-1})	Experiment (cm^{-1})	Experiment (cm^{-1}) [13]	Calculation (cm^{-1})	IR (calculation)	IR [13]	Experiment (cm^{-1}) [13]
631	637	625	645	Eg	A1g	630
606	615	605	577	B1g	B1g	**595**
570	559	554	471	B1g	Eg	465
521	536	534	456	Eg	Eg	410
505	503	500	?			305
477	476	476	**260**	**Eg**	**Eg**	**257**
382	387	392	188	B1g	B1g	**155**
344	347	334				
327	333	323				
309	305	297				
242	222	221				
204	191	193				
184	178	183				
128	100	115				

Table 5
Comparison between the Raman peaks (fitted using pseudo voigt functions), integrated intensities and FWMH measured on the non irradiated and 10^{15} Bi cm^{-2} sample. No significant shifts of the Raman peak and FWMH on the monoclinic phase are observed on these spectra. Under irradiation, the monoclinic Raman specter does not seem to be strongly perturbed. Only three extra peaks appear under irradiation and are similar to peaks associated to the tetragonal phase (cf. Table 4). Only one of these three peaks possesses an important integrated intensity

Sample irradiated by Bi atoms (10^{15} ion cm^{-2})			Non-irradiated sample		
Peak position (cm^{-1})	Normalized integrated intensity (%)	FWHM (cm^{-1})	Peak position (cm^{-1})	Normalized integrated intensity (%)	FWHM (cm^{-1})
102	37	9	101	27	10
164	4	31			
179	49	3	179	45	3
191	27	4	190	37	4
222	11	4	222	11	4
257	33	51			
306	21	9	306	18	10
334	61	6	334	39	6
343	27	7	348	37	8
383	39	12	384	56	9
387	50	4	387	27	4
392	32	4	392	26	4
475	100	9	475	100	10
502	20	8	502	15	8
537	21	9	537	13	9
559	17	12	559	36	12
586	**8**	**101**			
615	82	15	615	53	14
636	74.6	17	637	76	15

m → t phase transition occurs uniformly in the matrix during irradiation. Then the phase transition can be understood as an m → t phase transition. Moreover, no extra peaks different from the monoclinic and tetragonal phases nave been observed on irradiated samples. Then it seems that the mechanism responsible for the phase transitions is not an order–disorder mechanism.

3.3. Grazing X-ray diffraction on Bi implanted samples

The implantation of Bi and O ions in zirconia modifies the matrix creating interstitial atoms in a defined area. The atomic radius of O atoms is about 1.35 Å and is more or less equivalent to the atomic radius of Bi atoms (1.2 Å) [19]. The total atomic fraction of O

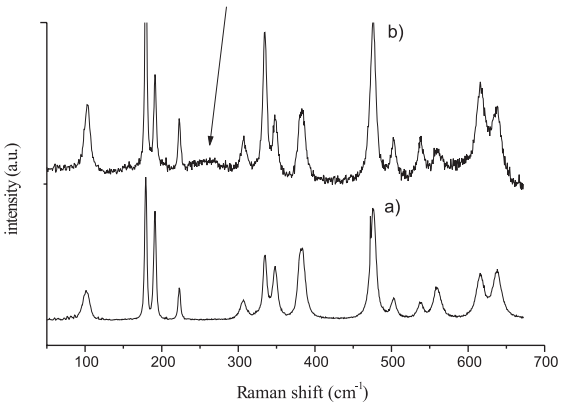

Fig. 7. Comparison of Raman spectra collected on non-irradiated zirconia sample (a) and implanted by 800 keV Bi ions with a fluence equal to 10^{15} ion cm^{-2} (b). On the irradiated sample, a wide broaden peak and two smaller peaks appear near 257, 164 and 586 cm^{-1} (cf. Table 5) as expected for the tetragonal phase (cf. Table 4). The other peaks collected on the sample b agree quite well with non-irradiated peaks (a). Then it seems that defects produced under irradiation do not modify the monoclinic phase. Moreover, no extra peaks other than peaks associated to monoclinic and tetragonal phases seems to appear during irradiation.

projectiles in zirconia is about 4.9×10^{-4} (for a fluence equal to 10^{15} O cm^{-2}). This value is superior to the atomic concentration of Bi atoms inducing the phase transition (10^{14} Bi cm^{-2}). Then the profile-implanted ions do not seem to induce the phase transition generating stress in the medium (cf. Figs. 5 and 6). In order to carefully confirm such an analysis and separate the effects due to the implanted profile and the dpa profile induced by atomic collisions, the average volumic tetragonal phase fraction is measured as a function of the incident angle using grazing X-ray on the most Bi implanted sample (cf. Appendix A).

Only one tetragonal [2] ($2\theta_{101t} = 30.17^{\circ}$) and two monoclinic [1] peaks ($2\theta_{-111m} = 28.17^{\circ}$ and $2\theta_{111m} = 31.5^{\circ}$) can be used to quantify the volumic fraction of each phase. No background evolution appears on the X-ray diffraction diagram associated to the most Bi irradiated sample. That means that no amorphisation of the material occurs. Moreover, all X-ray diffraction peaks can be indexed using the monoclinic and tetragonal phases only. Then we deduce that only two phases exist in these samples. We estimate the average local concentration of the tetragonal phase,

$$\langle c_t(x) \rangle = \frac{1}{x} \int_0^x c_\beta(u)\ \mathrm{d}u,$$

using only these three peaks. To minimise errors on the measured X-ray diffraction peaks, following Toraya [20], we create the function $q(x)$ as

$$q(x) = \frac{I_{101t}(x, \theta_{101t})}{I_{111m}(x, \theta_{111_m}) + I_{101t}(x, \theta_{101t}) + I_{-111m}(x, \theta_{-111m})} = \frac{\int_0^x c_t(u)\ \mathrm{d}u}{\int_0^x c_t(u)\ \mathrm{d}u + R(x) \int_0^x (1 - c_t(u))\ \mathrm{d}u},$$

with

$$R(x) = \frac{F_m^2(\alpha, 111) L(\theta_{111m}) + F_m^2(\alpha, -111) L(\theta_{-111m})}{F_t^2(101) L(\theta_{101t})}. \quad (1)$$

Such a formula is a good approximation to estimate the volumic fraction of the zirconia tetragonal phase induced by irradiation. To calculate the function $R(x)$ we neglect the variation of the Debye–Waller factor of the two phases and of the unit cell volume (equal to 70.1 $Å^3$ for the monoclinic phase and 70.6 $Å^3$ for the tetragonal phase). Using the integrated intensity allows one to neglect the spreading of intensities near points of the reciprocal lattice without a great mistake [10]. Then $R(x)$ become a constant equal to R. A Rietveld calculation using atomic parameters of Tewfer [2] permits to obtain the classical calculated structure factors F for each phase. R is equal to 1.75 for the Inel geometry and the Kα1 copper radiation. The average value $\langle c_t(x) \rangle$, in the $[0, x]$ slab, is obtained inverting Eq. (1).

Thirteen measurements at different grazing angles have been done on the most irradiated zirconia samples (by Bi projectiles with a fluence of 10^{15} ions cm^{-2}). Table 6 gives the probed depths, $\tau(\alpha)$, and the measured integrated intensities on this sample and Fig. 8 shows the evolution of the X-ray diffraction peaks of both the tetragonal and the monoclinic phases as a function of the incident angles. The melting point of zirconia T_m is 2973 K. Even if the local irradiation temperature is very difficult to measure, it is inferior to 0.2 T_m for the irradiation made at room temperature. Then it seems that defects due to dpa and implantation profiles do not diffuse and are similar to profiles calculated by TRIM-98.

Table 6
Integrated intensity values of the most Bi implanted sample as a function of the probed depth

Depth (Å)	$\langle c_q \rangle$	Absolute error
27	0.754	0.038
51	0.785	0.039
700	0.759	0.038
1137	0.746	0.037
1457	0.696	0.035
1806	0.671	0.034
2191	0.637	0.032
2488	0.635	0.032
2800	0.606	0.030
4180	0.504	0.025
5825	0.426	0.021
7232	0.351	0.018
8501	0.303	0.015

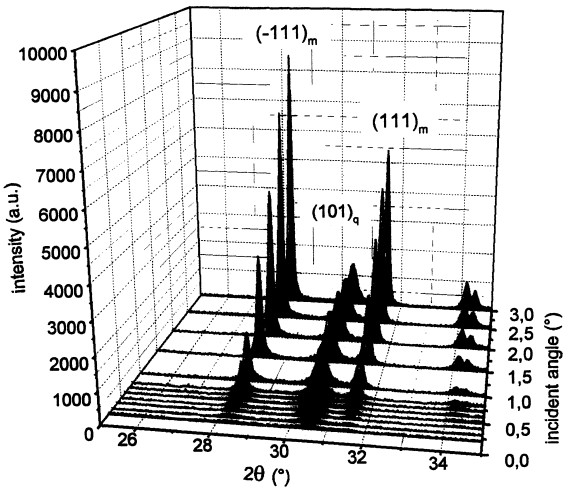

Fig. 8. Evolution of the average tetragonal phase as a function of the depth inside the most implanted zirconia samples (10^{15} Bi cm^{-2}) obtained using grazing X-ray diffraction with CuKα1 radiation.

X-ray diffaction leads only to measure the mean volumic fraction of the tetragonal phase and not the local one. Supposing that at each depth the local tetragonal volumic fraction is proportional to $D(x)$ (dpa profile) or $I(x)$ (implantation profile), we can calculate the function $\langle c_t(x)\rangle$ and compare it to the experimental values of $\langle c_t(x)\rangle$. Fig. 9 presents the shape of these two functions and compares them to the experimental $\langle c_t(x)\rangle$ profile. This comparison clearly shows that the measured average tetragonal phase can be understood as linked only to the dpa profile due to the ionic bombardment.

Fig. 10 shows the evolution of the average tetragonal phase as a function of the Bi fluence (10^{15} ions cm^{-2}).

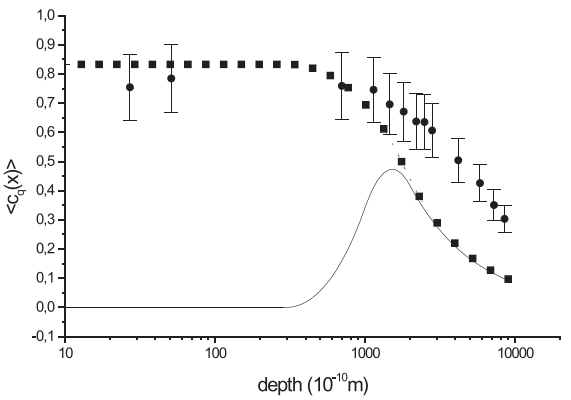

Fig. 9. Comparison between the experimental average zirconia tetragonal phase and the calculated average tetragonal phase obtained supposing that the local tetragonal phase is proportional to the deposed energy (dpa) profile (square) and the Bi implantation profile (line).

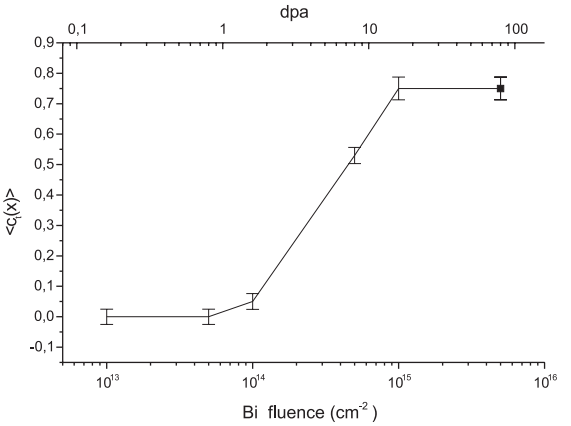

Fig. 10. Evolution of the average tetragonal phase as a function of the fluence of Bi implantation. The threshold fluence is equal to about 5×10^{13} Bi cm^{-2} (0.8 dpa). The last point at 5×10^{15} cm^{-2} (square) is obtained by analysis of Ref. [26]. A saturation effect appears clearly showing that the phase transition is not total.

This figure is obtained for an incidence equal to 0.3° (50 Å) to analyse effects induced only by dpa. Below 0.8 dpa (5×10^{13} ions cm^{-2}), no tetragonal phase appears. We then deduce that the dpa threshold measured at 303 K is equal to 0.8 (5×10^{13} ions cm^{-2}) dpa in our experiments, whereas this dpa threshold is equal to 5.9 dpa (5×10^{14} ions cm^{-2}) at 120 K for 340 keV Xe irradiation (dpa have been calculated in both cases using energy thresholds equal to 20 eV for Zr and 60 eV for O atoms). These results can be understood in the following way. The lower the temperature is, the lower the probability to create clusters. Then at low irradiation temperature, the number of dpa needed to obtain clusters is more important. According to these experiments, it seems then that the phase transition induced by irradiation is trigged by clusters (not yet observed by TEM). The effect of irradiation only seems to produce such clusters. For this reason, projectiles creating many cascades recovering (Bi and Xe ions) are more efficient to induce the phase transition than projectiles generating isolated or no cascades (O ions or electrons).

On irradiated samples (10^{15} Bi cm^{-2}) at all incident angles, Bragg angles have been measured and compared to theoretical Bragg angles associated to the monoclinic and tetragonal phases. The measured Bragg angles are shifted of 0.07° for the (−1 1 1) peak and 0.02° for the (1 1 1) peak. The Bragg shift (0.2°) observed on the tetragonal phase (1 0 1) can be understood as a compression of the tetragonal phase whereas the small shift observed on the monoclinic phase means that no stresses are present in the monoclinic phase. This result is in agreement with the published zirconia phase diagram, which shows that the high-pressure phase is the tetragonal

phase [21]. This description of such a compression of the quadratic phase is in agreement with the previous work of Sickafus et al. [8].

Because of the difficulty to separate monoclinic and tetragonal phases on the diffraction diagram, it was not possible to correctly plot any Williamson curves to study an eventual correlation between defects induced by irradiation using the broadening of X-ray diffraction peaks [22]. Because only one diffraction peak of the tetragonal phase is clearly defined, it was not possible to estimate any Debye–Waller factors associated to uncorrelated defects as a function of dpa using a Rietveld analysis.

4. Possible mechanism of the phase transition

To summarise the effects induced by ionic irradiation in zirconia, we can clearly say that an m → t phase transition generated by atomic collisions occurs. The tetragonal phase fits both experimental Raman and X-ray diffraction peaks. Even if complementary investigations have to be done, especially increasing the dpa values on zirconia irradiated by electrons and oxygen ions, some essential points describing the phase transition mechanism on pure monoclinic zirconia can be extracted from these experiments.

Neither a noticeable distortion of the X-ray diffraction peaks nor a sensitive modification of the X-ray background associated to the monoclinic and tetragonal phases as a function of dpa can be observed on samples irradiated by Bi ions. These facts associated to the absence of unidentified Raman peaks observed on irradiated zirconia seem to show that the phase transition is not an order disorder phase transition. In fact, correlated defects should broaden X-ray diffraction peaks and non-correlated defects must break down the Raman selection rules producing extra Raman peaks. All these facts lead us to think that clusters can be produced in zirconia during irradiation.

If we suppose that irradiation modifies the microstructure, generating clusters in cascades, the probability to create clusters depends on dpa and on the size of displacement cascades. Then the existence of these clusters could explains why dpa, for a given irradiation induced by an ion, is a good indicator of the phase transition. It could also explain the existence of a dpa threshold below which no phase transition occurs. If we suppose the existence of clusters induced by irradiation, many different mechanisms can induce the phase transition.

Clusters could compress the monoclinic phase [23], and such a local compression could be responsible of the phase transition with the apparition of the tetragonal phase in agreement with the phase diagram [21]. Following Friedel [24], it is possible to calculate the elastic energy due to an isolated cluster in the matrix. This energy can be roughly calculated as:

$$E \approx 6c\mu\Omega f^2,$$

where Ω is the unit cell volume, μ the shear modulus, c the cluster concentration and f is the size factor.

The analysis of the X-ray diffraction permits to choose the size factor as the reticular variation associated to the Bragg angle shift observed on the tetragonal phase (6.3×10^{-3}). If the compression due to such clusters induces the phase transition, the elastic energy stored is at least equal to the difference between cohesion energies of the two phases (about 0.1 eV) [25]. The cluster concentration calculated is too important.

Because a clear compatibility relation exists between space groups associated to the tetragonal (D_{4h}^{15}) and monoclinic (C_{2h}^{5}) phases, a group theoretical calculation proves that the phase transition of tetragonal zirconia as a function of temperature is due to phonon soft modes associated to oxygen anion movements in the crystal [6]. On irradiated samples, clusters produced by irradiation may modify these soft modes which trig the monoclinic tetragonal phase transition. The analysis of Raman spectra of the most irradiated Bi–zirconia sample seems to confirm such an hypothesis. In fact, the 257 cm^{-1} Raman peak associated to the oxygen shell embedded zirconium ions becomes a band on irradiated sample. Only this peak presents such a broadening in agreement with clusters apparition during irradiation (cf. Table 5).

5. Conclusion

This work extended previous studies of zirconia behaviour under irradiation using a Raman microprobe (short range order probe) and a grazing X-ray diffraction non-local probe (long range order probe) to analyse the cell evolution of the pure monoclinic zirconia under different kinds of irradiations (electrons, Bi^{2+} and O^{2+} ions). The association of these methods shows the evidence of an m → t phase transition under irradiation. The new phase created by irradiation is clearly the tetragonal phase. Moreover, the transition is controlled by a dpa threshold. The proposed elementary mechanism of the transition is the formation of clusters during the ballistic collision. Different shifts observed on grazing X-ray diffraction diagrams show that the tetragonal phase is compressed, whereas the surviving monoclinic phase is not affected by clusters produced during irradiation. The fact that only one Raman peak associated to the tetragonal phase is broadened shows that the perturbation due to cluster may act on phonons soft modes.

Therefore these analyses are not sufficient to build a more precise description of the phase transition induced by irradiation explaining for instance the high stability

of the stabilised zirconia phases under irradiation. Many points have to be confirmed and complementary analyses are in progress in our laboratory to assess the phase transition mechanism presented in this paper.

Acknowledgements

It is a pleasure to thank Professor C. Lemaignan and Professor D. Lesueur for helpful discussions during the various stages of this work. We acknowledge M. Plantier for the irradiation of zirconia samples by ions and M. Ardonceau for the irradiation of zirconia samples by electrons.

Appendix A

The intensity of the fraction of a phase β, c_β, collected at depth x by the detector can be written as [17]

$$I_\beta(\theta,\alpha,x) = AF^2(\alpha,hkl)|L(\theta)| \int_0^\infty \exp(-ay)c_\beta(x-y)\ \mathrm{d}y = B(\theta,\alpha)\int_0^\infty \exp(-a(2\theta)y)c_\beta(x-y)\ \mathrm{d}y, \tag{A.1}$$

where A is a geometric factor, F the pseudo-structure factor averaged over crystallographic direction associated to the Bragg angle θ, L the Lorentz polarisation correction, $c_\beta(x)$ the concentration of the phase β at the depth x and $a(2\theta)$ the absorption coefficient linked to the linear absorption coefficient associated to the mixing of two phases. $a(2\theta)$ can be written as

$$a(2\theta) = \mu_m\left(\frac{1}{\sin\alpha} + \frac{1}{\sin(2\theta-\alpha)}\right) \tag{A.2}$$

(the output angle after the refraction on the surface α_s is equal to α in the grazing incidence), where μ_m is the linear absorption coefficient of the mixture.

The Lorentz polarisation factor for the Inel geometry is

$$L(\theta) = \cos(2\theta-\varphi)\frac{1}{\sin 2\theta\sin(2\theta-\varphi)\cos(\theta)} \times\left(\frac{1+\cos^2 2\theta}{2}\right). \tag{A.3}$$

In the geometrical condition of the X-ray collected spectra, $a(2\theta)$ does not depend of $\theta(a(2\theta)\approx a)$ and for this study, we have typically analysed depths which are always inferior to 2 μm. Moreover, the linear absorption coefficient associated to each phase of zirconia is equal to 600 cm^{-1} for the CuKα1 radiation. This implies that $\exp(-a(2\theta)(x-u))$ is equal to 1 with a precision inferior to 12% in our experiments. Then the intensity I_β obtained for a depth x can be linked to the concentration of the phase β by

$$I_\beta(\theta,\alpha,x) = B(\theta,\alpha,x)\int_0^x c_\beta(u)\ \mathrm{d}u. \tag{A.4}$$

References

[1] C. Howard, R. Hill, B. Reichert, Acta Crystallogr. B 44 (1988) 116.
[2] G. Tewfer, Acta Crystallogr. 15 (1962) 1187.
[3] R. Wychoff, Cryst. Struct. 1 (1963).
[4] E. Subbarao, H. Haiti, K. Srivastava, Phys. Stat. Solidi A 21 (1974) 9.
[5] K. Negita, Acta Metall. 37 (1) (1989) 313.
[6] K. Negita, H. Takao, J. Phys. Chem. Solid 50 (3) (1989) 325.
[7] H. Boysen, F. Frey, T. Vogt, Acta Crystallogr. B 47 (1991) 881.
[8] K. Sickafus, K.H. Matzke, T. Hortmann, K. Yasuda, J. Valdez, P. Chodak, H. Nastasi, R. Verrall, J. Nucl. Mater. 274 (1999) 66.
[9] G. Vineyard, Phys. Rev. B 26 (8) (1982) 4146.
[10] M. Brunel, F. De Bergevin, Acta Crystallogr. A 42 (1986) 299.
[11] T. Hirata, E. Asari, M. Kitajima, J. Solid State Chem. 110 (1994) 201.
[12] M. Ishigame, T. Sakurai, Phys. Stat. Solidi 203 (1997) 557.
[13] M. Ishigame, T. Sakurai, J. Am. Ceram. Soc. 60 (1976) 367.
[14] S. Zinkle, C. Kinoshita, J. Nucl. Mater. 251 (1997) 200.
[15] A. Tawfik, M. Abd El Ati, F. Ashry, M. Sekhina, J. Phys. Soc. Jpn. 54 (8) (1985) 3012.
[16] A. Mirgorodsky, M. Smirnov, P. Quintard, J. Phys. Chem. Solid 60 (7) (1999) 985.
[17] H. Shannon, Acta Crystallogr. A 32 (1976) 751.
[18] E. Kisi, C. Howard, Key Eng. Mater. 153&154 (1998).
[19] B. Cullity, Elements of X-ray diffraction, Addison Wesley, Wokingham, UK, 1979.
[20] M. Toraya, M. Yoshimura, S. Somiya, J. Am. Ceram. Soc. C 119 (1984).
[21] J. Leger, P. Thomazewski, A. Atouf, A. Perreira, Phys. Rev. B 47 (21) (1993) 1475.
[22] D. Simeone, D. Gosset, D. Quirion, X. Deschanels, J. Nucl. Mater. 264 (1999) 295.
[23] R. Averback, T. Diaz de la Rubia, Solid State Phy. 51 (1997) 281.
[24] J. Friedel, Philos. Mag. 46 (1955) 514.
[25] G. Jomard, T. Petit, A. Pasturel, L. Magaud, G. Krese, J. Hafner, Phys. Rev. B 59 (6) (1999) 4044.
[26] F. Brossard, thesis, University Claude Bernard Lyon I, France, 1999.